

# Single Ag Nanoparticle Collisions within a Dual-Electrode Micro-Gap Cell

Kim McKelvey,<sup>1,2,\*</sup> Donald A. Robinson,<sup>1</sup> Nicholas J. Vitti,<sup>1</sup> Martin A. Edwards,<sup>1</sup> Henry S. White<sup>1,\*</sup>

<sup>1</sup>Department of Chemistry, University of Utah, Salt Lake City, UT 84112

<sup>2</sup>School of Chemistry, Trinity College Dublin, Dublin 2, Ireland

Corresponding authors: \*[kim.mckelvey@tcd.ie](mailto:kim.mckelvey@tcd.ie), \*[white@chem.utah.edu](mailto:white@chem.utah.edu)

## Contents

S1: Optical Image of Electrode Alignment .....	S2
S2: Alternating Current(AC) SECM Configuration .....	S3
S3: Constant-Height AC-SECM Scan for Electrode Alignment.....	S4
S4: AC-SECM Approach Curve.....	S5
S5: Negative Feedback Approach Curve .....	S6
S6: Finite Element Simulations .....	S7
S7: Capacitive Coupling as a Function of Gap Width .....	S9
S8: Ag Nanoparticle Oxidation in a Micro-gap Cell with Both Electrodes at Oxidizing Potentials .....	S10
S9: Ag Nanoparticle Oxidation in a Micro-gap Cell Formed by Two Equal-Sized Electrodes with Both at Oxidizing Potentials .....	S11
S10: Oxidation Event Spanning Two Electrodes .....	S12
S11: Oxidation Charge vs Gap Distance .....	S13

S1. Optical Image of Electrode Alignment.

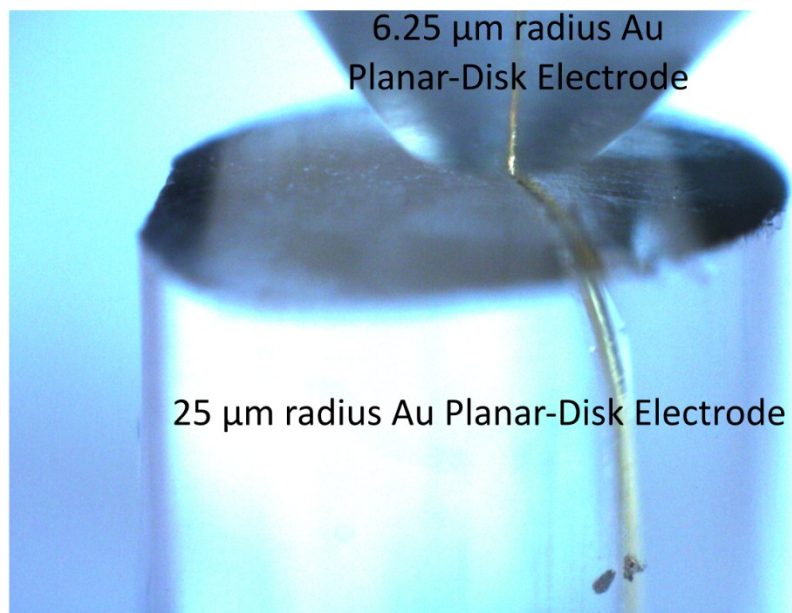


*Figure S1: Optical image of electrode alignment showing the smaller 6.25  $\mu\text{m}$  radius Au electrode on the top and the larger 25  $\mu\text{m}$  radius Au electrode on the bottom. The 6.25  $\mu\text{m}$  radius top electrode is typically used as the oxidation electrode, while the bottom 25  $\mu\text{m}$  electrode is typically used as the collection electrode. Image taken in air, prior to the addition of electrolyte.*

S2: Alternating Current(AC) SECM Configuration

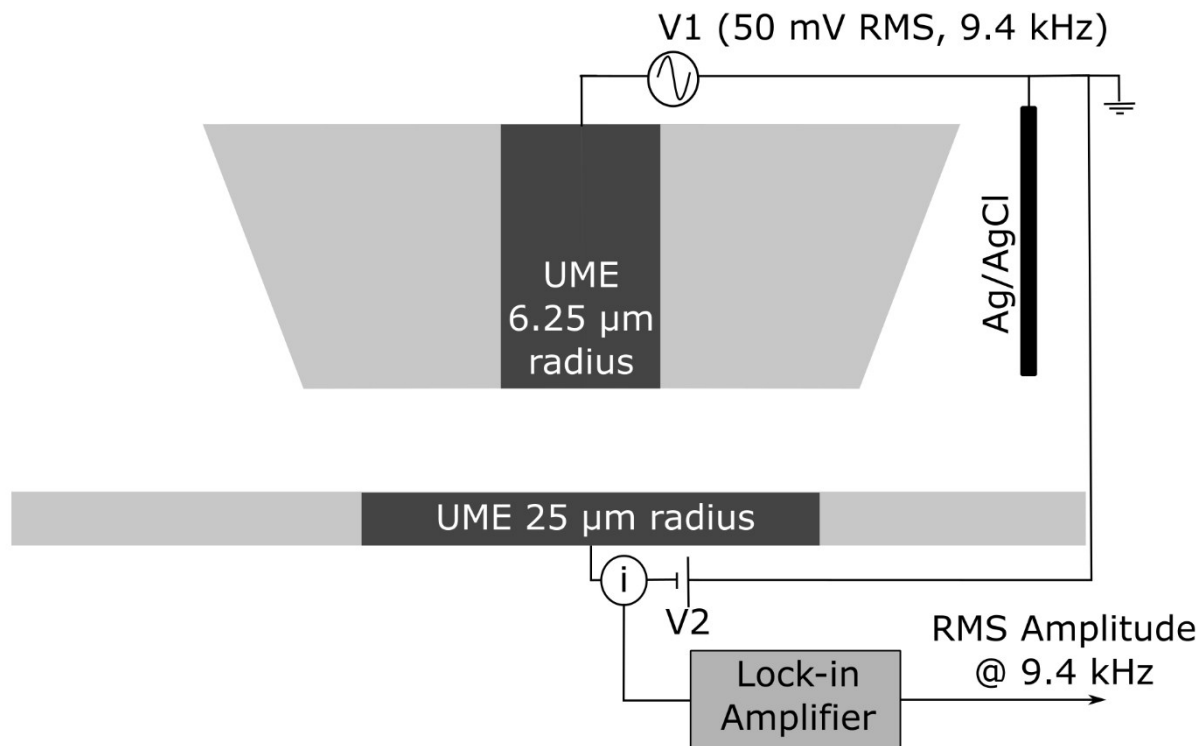


Figure S2: Diagram of AC-SECM configuration (not drawn to scale) showing the AC potential applied to the top/oxidation electrode and the induced oscillation current measured at the bottom/collection electrode.

### S3: Constant-Height AC-SECM Scan for Electrode Alignment

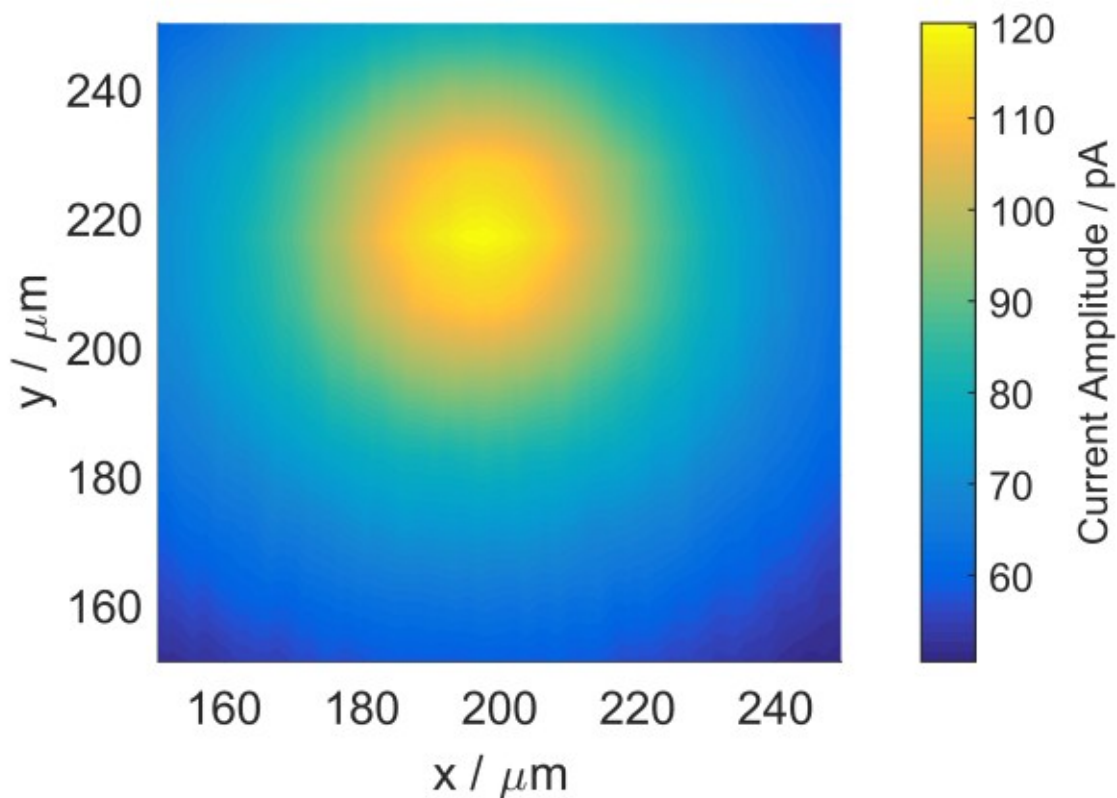


Figure S3: Constant height AC-SECM scan of the induced current oscillation (RMS amplitude) on the bottom/collection ( $25\ \mu\text{m}$  radius) electrode as a function of the position ( $x$ ,  $y$ ) of the top/oxidation ( $6.25\ \mu\text{m}$  radius) electrode with an approximate vertical electrode separation of  $25\ \mu\text{m}$  in  $20\ \text{mM KNO}_3$ . Optimal alignment of the two electrode is defined as the position where the current oscillation amplitude is maximal ( $x = 195\ \mu\text{m}$ ,  $y = 218\ \mu\text{m}$ ).

#### S4: AC-SECM Approach Curve

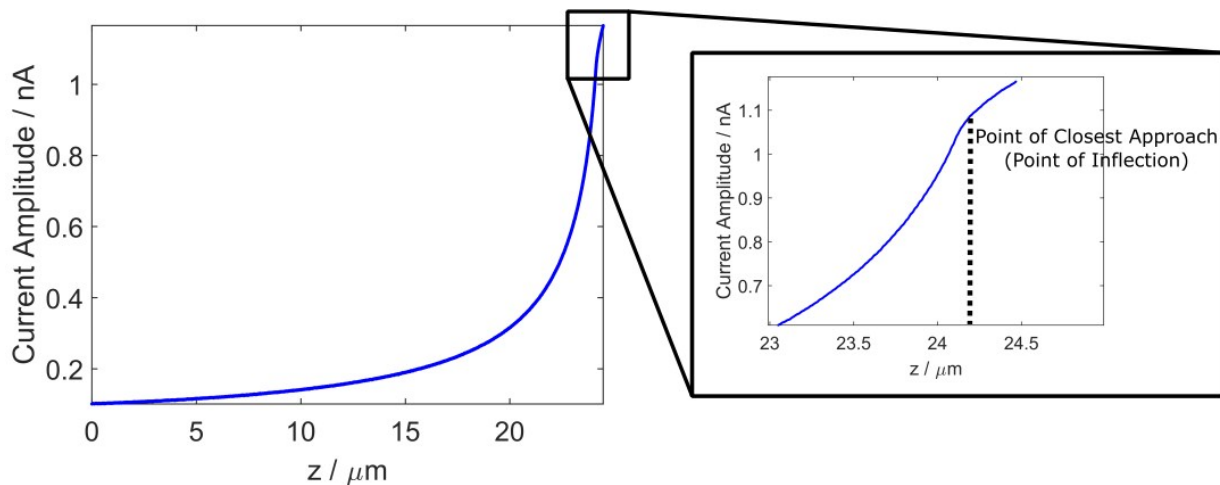


Figure S4: AC-SECM approach curve, showing the RMS amplitude of the current oscillation at the bottom/collection electrode (a  $25 \mu\text{m}$  radius planar disk) as the top/oxidation electrode ( $6.25 \mu\text{m}$  radius planar disk) is moved toward it (initial position  $z = 0 \mu\text{m}$ ) in  $20 \text{ mM KNO}_3$ . The point of closest approach is determined by the point of inflection in the approach curve, labelled in the insert to the right at  $24.18 \mu\text{m}$ . The current amplitude at the bottom/collection electrode was measured at  $9.4 \text{ kHz}$  and induced by a  $50 \text{ mV (RMS)}$   $9.4 \text{ kHz}$  potential applied to the top/oxidation electrode.

## S5: Negative Feedback Approach Curve

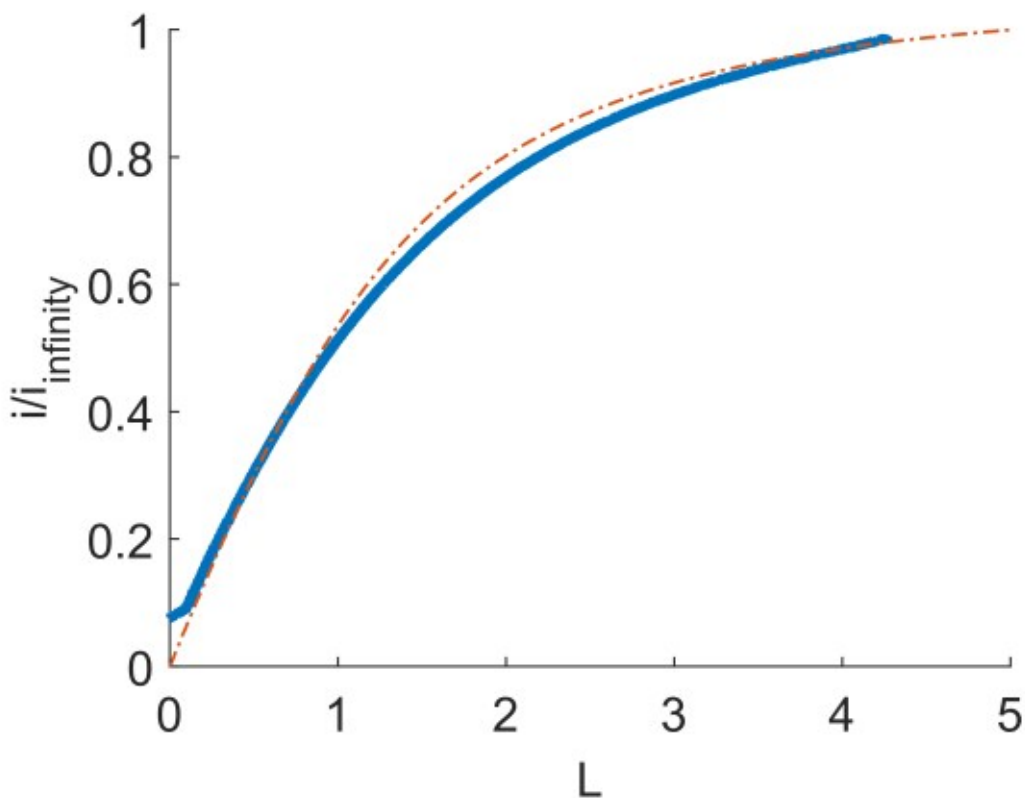


Figure S5: Blue line: experimentally measured negative approach curve for the 6.25  $\mu\text{m}$  radius (with 100  $\mu\text{m}$  surrounding glass) electrode to an insulating glass surface (the glass electrode sheath of the larger 25  $\mu\text{m}$  radius electrode) in 3 mM hexaammineruthenium(III) chloride 20 mM  $\text{KNO}_3$  and 2 mM trisodium citrate ( $\text{Na}_3\text{C}_6\text{H}_5\text{O}_7$ ). The hexaammineruthenium(III) reduction current is normalized by  $i_{\text{infinity}}$ , the hexaammineruthenium(III) reduction current measured with the electrode far from the surface and the distance is divided by the electrode radius,  $a$  ( $L=z/a$ ). Red dashed line: theoretical response for a negative approach curve to an insulating surface ( $RG = 16$ ).<sup>1</sup> At the point of closest approach (i.e., the point of inflection on the blue approach curve) the normalized current is 0.1 and therefore the point of closest approach is ca. 600 nm.

## S6: Finite Element Simulations

Time-dependent 2D axisymmetric finite element simulations were used to describe the diffusive transport of  $\text{Ag}^+$  following the oxidation of a single Ag nanoparticle. COMSOL Multiphysics (version 5.2a) was used to perform the simulations, which were run on a desktop PC.

The transport of  $\text{Ag}^+$  in the nanogap was described as a diffusion process using Fick's second law, which is given by:

$$\frac{\partial c}{\partial t} = D \nabla^2 c,$$

where  $c$  is the concentration of  $\text{Ag}^+$  and  $D$  is the diffusion coefficient of  $\text{Ag}^+$  which is set to  $1.6 \times 10^{-5} \text{ cm}^2/\text{s}$ .<sup>2</sup>

### *Simulation Domain*

The 2D axisymmetric simulation domain comprising the nanoparticle, oxidation electrode and collection electrode is shown in Figure S6 A. The initial concentration of  $\text{Ag}^+$  was set to zero everywhere in the simulation domain except inside the nanoparticle where it was set to 97.2 M (based on a density of Ag of  $10.49 \text{ g/cm}^3$  and Ag molecule weight of  $107.86 \text{ g/mol}$ ), as shown in Figure S6 A. The concentration of  $\text{Ag}^+$  at the bulk boundaries was set to 0, as was the concentration of  $\text{Ag}^+$  at the collection electrode surface, as shown in Figure S6. All other boundaries were set as no flux boundaries. The gap width was set values between 600 nm and  $20 \text{ }\mu\text{m}$  (with a step size of  $1.5 \text{ }\mu\text{m}$  between each simulation). No change in the collector electrode geometry, due to the deposition of Ag, was considered.

To aid the simulation stability, for the first 10 ms a thin diffusion barrier boundary around the nanoparticle contains the  $\text{Ag}^+$  inside the nanoparticle. Over the next 20 ms the thin-layer is smoothly removed to simulate the dissolution of the entire nanoparticle. A high-density mesh at the boundary of the nanoparticle, as shown in Figure S6, was used. The collection current was calculated by integrating the normal  $\text{Ag}^+$  flux across the collection electrode boundary.

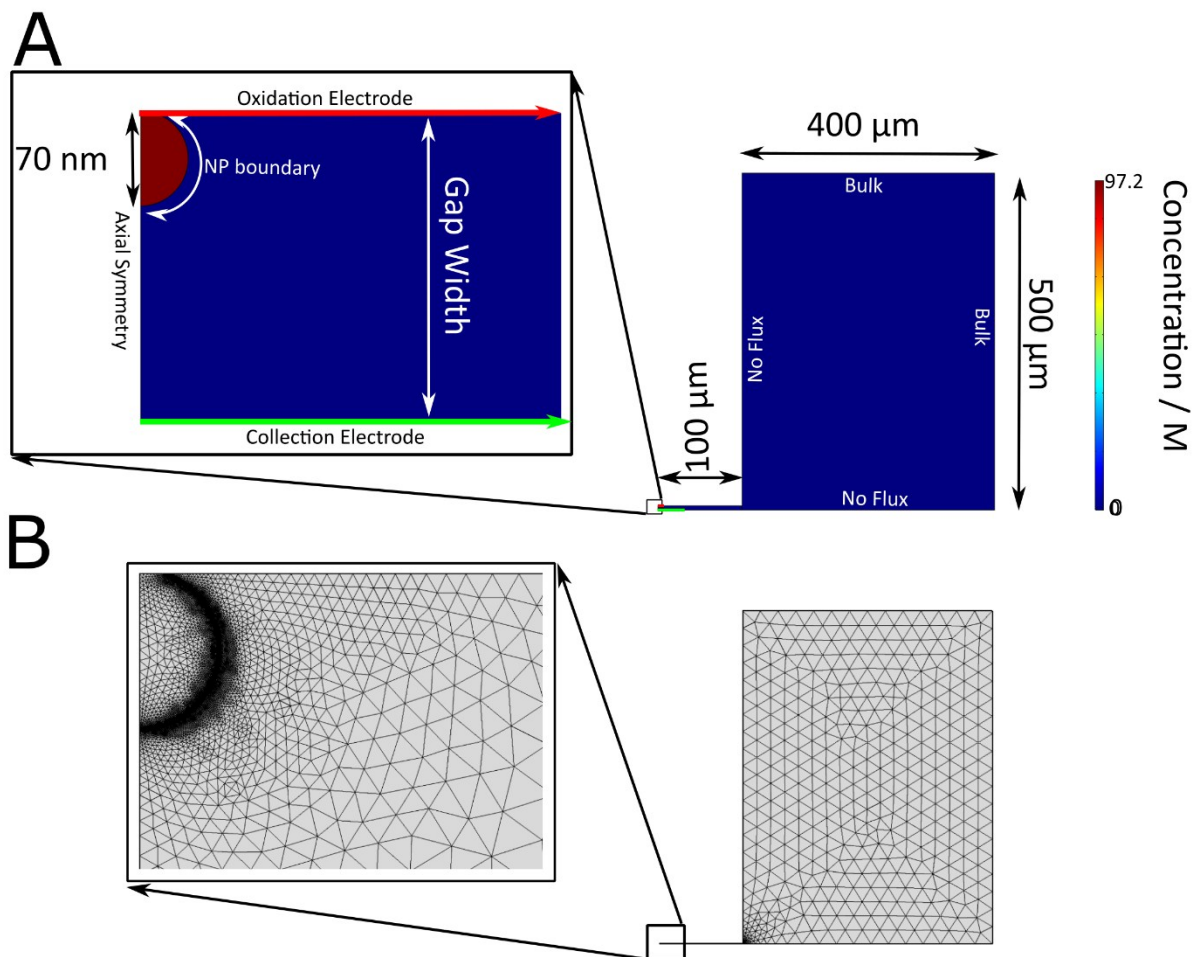


Figure S6: Simulation domain (A) and mesh (B) for the nanoparticle dissolution simulation.



## S7: Capacitive Coupling as a Function of Gap Width

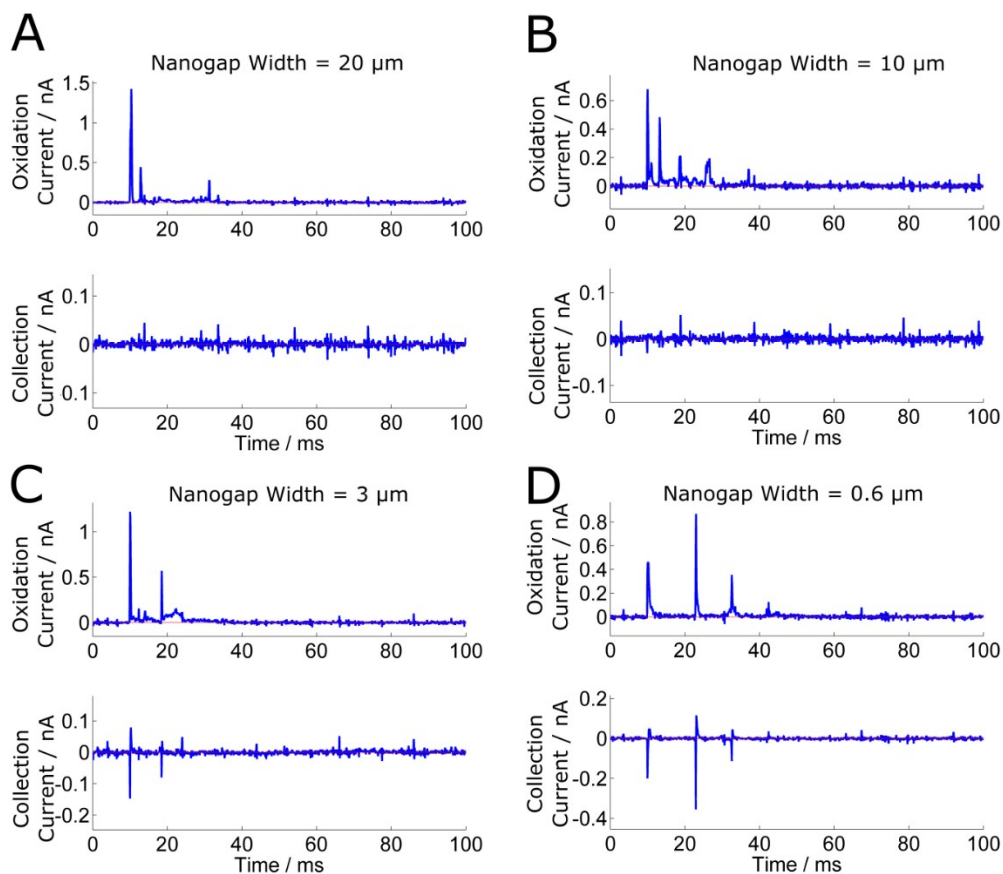
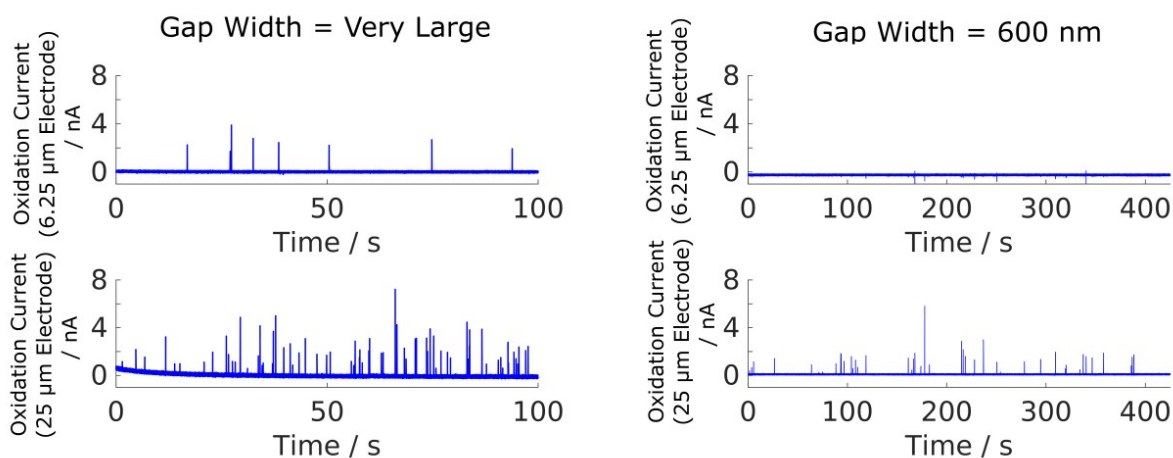


Figure S7: Capacitive coupling on the second electrode (6.25  $\mu\text{m}$  radius Au planar disk, 750 mV vs Ag/AgCl (sat. KCl), lower trace in each section) upon the multiplexed oxidation of a single Ag nanoparticle on the oxidation electrode (6.25  $\mu\text{m}$  radius Au planar disk, 750 mV vs Ag/AgCl (sat. KCl), top traces in each section) with a gap distance of **A.** 20  $\mu\text{m}$ , **B.** 10  $\mu\text{m}$ , **C.** 3  $\mu\text{m}$  and **D.** 600 nm in a 20 mM  $\text{KNO}_3$  (Sigma-Aldrich) and 2 mM trisodium citrate solution. Note that in this configuration oxidation events were observed on both electrodes, as both electrodes are identical in size and both held at oxidizing potentials. However only a selection of 4 individual collision events at different gap widths and with the oxidation occurring on the top electrode are shown here.

## S8: Ag Nanoparticle Oxidation in a Micro-gap Cell with Both Electrodes at Oxidizing Potentials



*Figure S8. Oxidation current-time traces for the oxidation of single Ag nanoparticles on two aligned planar-disk electrodes both held at 850 mV vs Ag/AgCl (sat. KCl), one 6.25  $\mu\text{m}$  radius and the other 25  $\mu\text{m}$  radius, with a gap of either very large ( $>20 \mu\text{m}$ ) (left) or 600 nm (right) between the electrodes. Note the different duration of the two current traces. When the electrodes are separated by a large distance ( $> 20 \mu\text{m}$ ) the frequency of collisions on the larger electrode is 8 times greater than on the small electrode (8 collision in 100 seconds compared to 67 collisions in 100 seconds). However, when the gap is reduced to 600 nm, oxidations are only observed on the larger electrode, although a variable capacitance coupling current is observed at the 6.25  $\mu\text{m}$  radius electrode. This occurs due to the narrow gap between the electrode sheaths increasing the likelihood that the particle first encounters the outer part of the larger electrode; oxidation of the particle then prevents it reaching the smaller electrode. Moreover, the narrow gap also decreases the frequency of collisions on the large electrode (41 in 425 seconds = 0.096 Hz with a gap distance of 600 nm compared to 67 in 100 seconds = 0.67 Hz for a very large ( $>20 \mu\text{m}$ ) gap distance).*

S9: Ag Nanoparticle Oxidation in a Micro-gap Cell Formed by Two Equal-Sized Electrodes with Both at Oxidizing Potentials

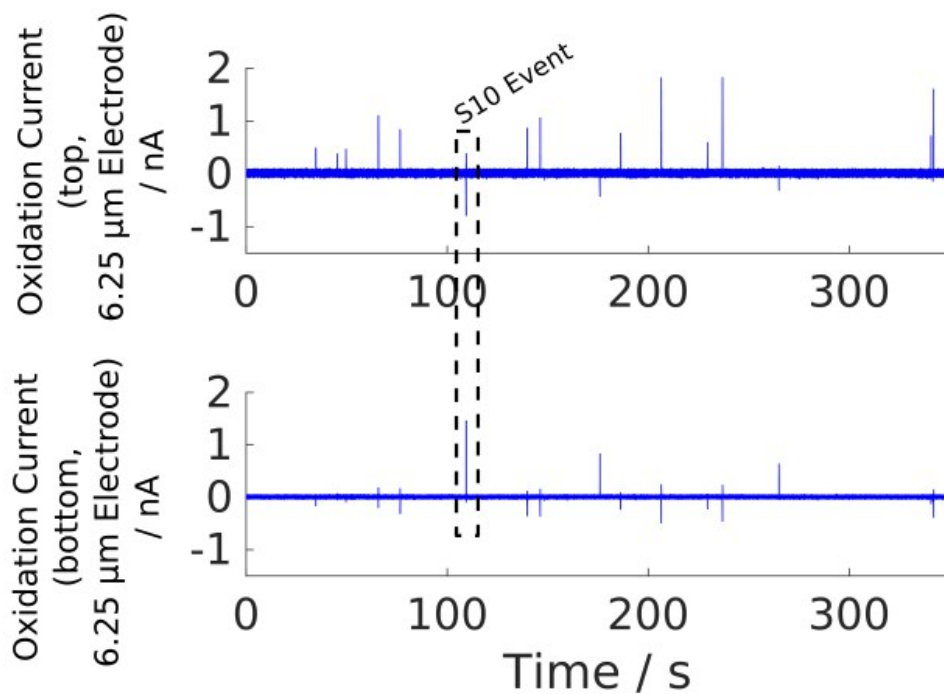


Figure S9. Current-time traces for Ag nanoparticle oxidation on two aligned 6.25  $\mu\text{m}$  radius electrodes, each held at 750 mV vs Ag/AgCl and separated by a gap of 600 nm. Oxidation events are observed at each electrode where corresponding coupling currents are observed on the other electrode. The collision event shown in S10, which spans the two electrodes, is marked.

## S10: Oxidation Event Spanning Two Electrodes

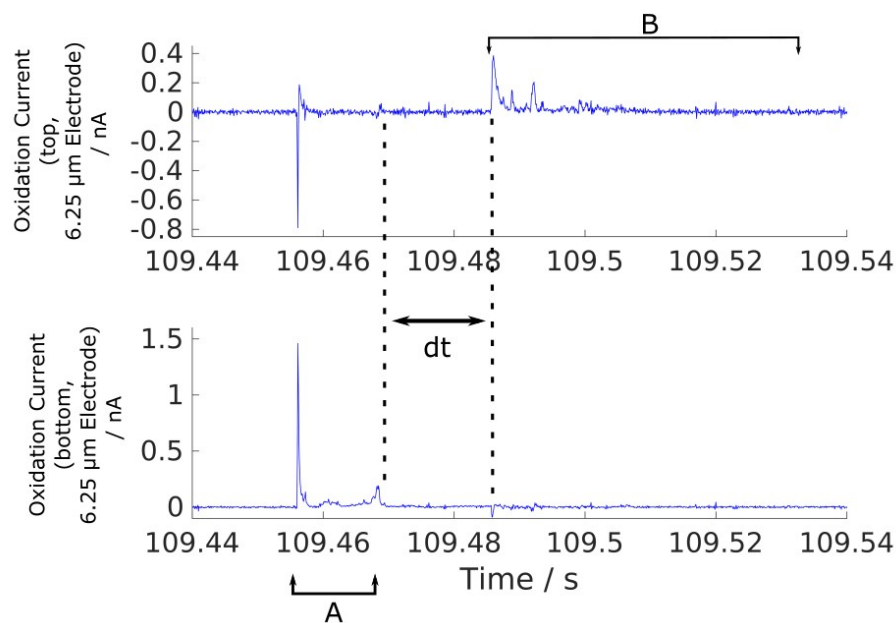


Figure S10. Oxidation of a single nanoparticle spanning two aligned  $6.25 \mu\text{m}$  radius planar disk electrodes, both held at  $750 \text{ mV}$  vs  $\text{Ag}/\text{AgCl}$ . Event marked in the longer time-current trace in Figure S9. The section labelled A shows the oxidation of the nanoparticle on the bottom electrode, and a short time ( $dt$ ) later the oxidation continues on the top electrode, which is labelled as section B. Note that a capacitive coupling current is observed on the electrode not responsible for oxidizing the nanoparticle (i.e., on the top electrode in section A and on the bottom electrode in section B). The time it takes for the single nanoparticle to diffuse from the bottom electrode to the top electrode is  $17 \text{ ms}$ , labelled as  $dt$  above. Based on the Stokes–Einstein equation, the diffusion coefficient for a  $35 \text{ nm}$  radius nanoparticle in an aqueous solution is  $7 \times 10^{-8} \text{ cm}^2 \text{ s}^{-1}$ , which gives a characteristic diffusion time across a  $600 \text{ nm}$  gap of  $t = L^2/2D = (600 \text{ nm})^2 / (2 \times 7 \times 10^{-8} \text{ cm}^2/\text{s}) = 25 \text{ ms}$ , in close agreement with the experimentally measured value. The total oxidative charge for the single nanoparticle is  $1.9 \text{ pC}$  (with  $1.1 \text{ pC}$  passed through the bottom electrode and  $0.8 \text{ pC}$  passed through the top electrode) which compares with the theoretical charge for a single  $35 \text{ nm}$  radius  $\text{Ag}$  nanoparticle of  $1.7 \text{ pC}$ .

### S11: Oxidation Charge vs Gap Distance

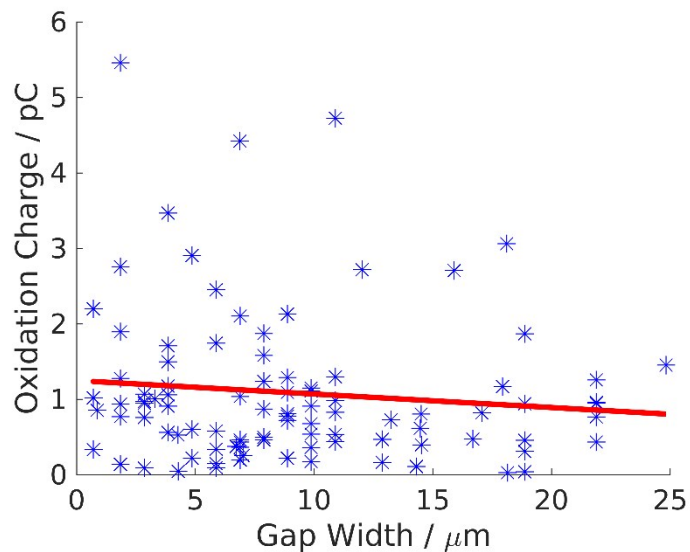


Figure S11: Oxidation charge as a function of gap width, showing a slight trend for increasing oxidation charge with a decrease in the gap width. The oxidation electrode (6.25  $\mu\text{m}$  radius, 100  $\mu\text{m}$  of surround glass sheath) is held at a potential of 750 mV, while a collection electrode (25  $\mu\text{m}$  radius) was held at -150 mV.

#### References:

- (1) *Electroanalytical Chemistry: A Series of Advances: Volume 26*; Bard, A. J., Zoski, C. G., Eds.; CRC Press, 2015.
- (2) *CRC Handbook of Chemistry and Physics*, 90th ed.; Lide, D. R., Ed.; CRC Press/Taylor and Francis: Boca Raton, FL, 2009.